Supplementary Information

Nanoscale magnetic and charge anisotropies at manganite interfaces

Santiago J. Carreira,[a,b] Myriam H. Aguirre,[c,d,e] Javier Briatico,[f] and Laura B. Steren,[a,b]

[a.] Consejo Nacional de Investigaciones Científicas y Técnicas, Argentina. Tel: 54-11 6772-7103; E-mail: steren@*tandar.cnea.gov.ar.*
[b.] Laboratorio de Nanoestructuras Magneticas y Dispositivos. Dpto. Materia Condensada e Instituto de Nanociencia y Nanotecnología (INN), Centro Atómico Constituyentes (CNEA), 1650 San Martín, Buenos Aires, Argentina.
[c.] Instituto de Ciencia de Materiales de Aragón (ICMA) e Instituto de Nanociencia de Aragón (INA), Universidad de Zaragoza, E-50018 Zaragoza, Spain. Fax: +34 976 76 2776; Tel: +34 876 55 5365; E-mail: maguirre@unizar.es.
[d.] Departamento de Física de la Materia Condensada, Universidad de Zaragoza, E-50009 Zaragoza, Spain.
[e.] Laboratorio de Microscopías Avanzadas, Universidad de Zaragoza, E-50018 Zaragoza, Spain.
[f.] Unité Mixte de Physique, CNRS, Thales, Université Paris-Sud, Université Paris-Saclay, Palaiseau 91767, France.

1. Overall structural properties

The crystalline structure and thickness of the bilayers was characterized with standard x-ray reflectivity and x-ray diffraction scans for both sample'series and complemented with cross sectional transmission electron microscopy images and GPA analysis. Fig. S1(a) shows the typical x-ray reflectivity scan obtained for the bilayers, where kiessig fringes are clearly observed until large angles, signaling the high surface quality of the samples. In Fig. S1 we show typical x-ray patterns at (002) Bragg reflection, where the (002) peaks related to the $LS_{0.3}MO$ are found closed to the substrate peaks. No other peaks were found apart from the (00n), as expected for an epitaxial and coherent growth oriented along the [001] axis.

XRD measurements were used to assess quantitatively and accurately the out-of-plane parameters of the $LS_{0.3}MO$ bottom electrode. The out-of-plane lattice parameters and the *c/a* ratio of the capping layers were calculated from the (002) Bragg peak, assuming that the in-plane lattice parameters remain constant at the $SrTiO_3$ lattice parameter, a = 3.905 Å. It is noteworthy to mention that the *c/a* ratio calculated from the XRD experiments for the $LS_{0.3}MO$ agrees with the one derived from GPA analysis.The structure of the $LS_{0.3}MO$ inner layers for both series is tensile strained with $c < a$. whereas the unit cell of the LS_xMO outer layers is elongated along the [001] axis, where $c > a$. The Bragg peak relative to the LS_xMO could not be resolved from the XRD scans owing to their low intensity and their proximity to the substrate peak.

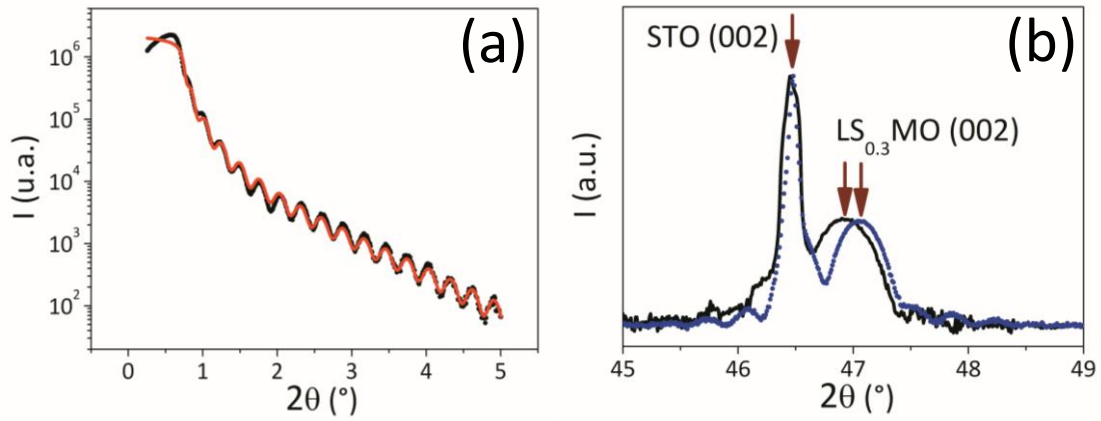

Fig. S1: (a) x-ray reflectivity of a typical sample and (b) x-ray diffraction scans at the (002) Bragg reflection for the (line) LMO (4.7 nm)/$LS_{0.3}MO$//STO (4.7-LMO) and (dots) $LS_{0.1}MO$ (5.9 nm)/$LS_{0.3}MO$//STO (5.9-$LS_{0.1}MO$) samples.

Reflection high-energy electron diffraction (RHEED) is sensitive to surface structure and surface roughness and can be used to define the surface morphology of a growing thin film [S1]. The RHEED pattern at room temperature prior to the growth consists of spots on the 0th-order Laue circle, corresponding to the intersection of the Ewald sphere and the reciprocal lattice, and indicates a smooth surface. In contrast to the spots observed for the $SrTiO_3$ shown in Fig. S2(a), we observe in Fig. S2(b) diffuse lines for the sample surface, signaling the existence of small terraces. The similarity of both patterns lead us to conclude that the surface features is conserved after growth and the surface termination of the films is indeed MnO_2 [S2].

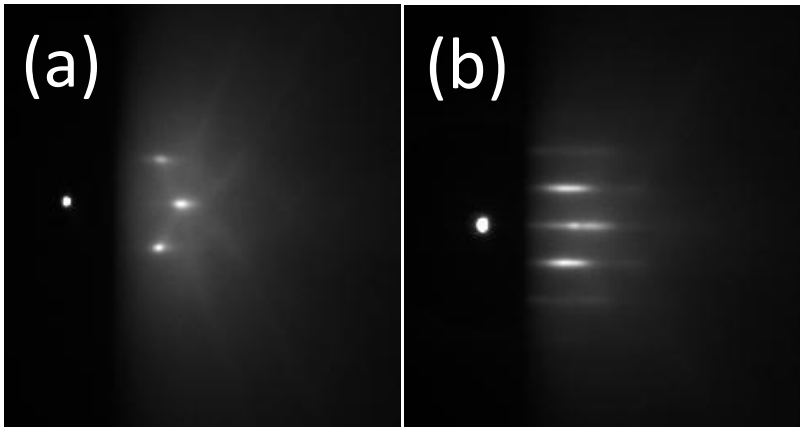

Fig. S2: RHEED pattern taken with the incident beam along $SrTiO_3$ [100] of (a) a TiO_2-terminated $SrTiO_3$ substrate prior to deposition and (b) one of the bilayers after deposition.

2. Magnetic anysotropies of the bilayers

In magnetic materials, the absorption of linearly polarized x-rays is sensitive to the charge anisotropy of the probes ions (preferential orbital filling) and the spin orientation of ferromagnetic and antiferromagnetic phases. The ferromagnetic component can easily be oriented with an external magnetic field parallel to incident polarized radiation (perpendicular to the electric field vector), keeping the antiferromagnetic spin axis invariant due to their stronger magnetic anisotropy with respect to the ferromagnetic part. As a result, the ferromagnetic contribution can be canceled out from the x-ray linear dichroism (XLD) signal by applying a magnetic field parallel to the incident polarized radiation. Bearing these considerations in mind, we characterized the overall magnetic properties of the bilayers with standard magnetization measurements. The hysteresis loops shown in Fig. S3 measured with the magnetic field applied perpendicular to the sample plane show a hard magnetic axis in the [001] direction, where a magnetic field of 1T is required to reach the saturation magnetization of the ferromagnetic component. This magnetic field will be enough to get ride from the ferromagnetic contribution on the XLD signal and probes only the antiferromagnetic component.

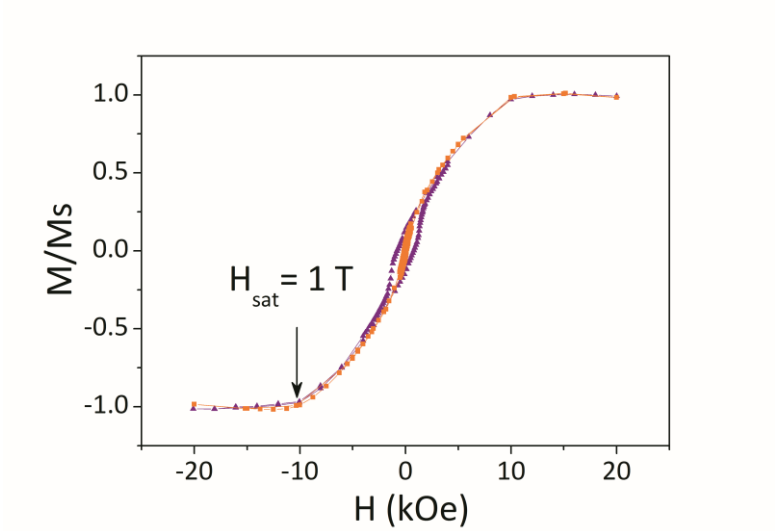

Fig. S3: Hysteresis loops measured at 10 K with the magnetic field applied parallel to the [001] axis for the samples 5.9-$LS_{0.1}$MO (circles) and 4.7-LMO (triangles).

3. Magnetization reversal process. In-plane hysteresis cycles

In Fig. S4 we show the hysteresis cycles obtained at 4 K for one sample of the t-LMO series, where the magnetic field was applied parallel to the sample plane. All samples were cooled down in absence of a magnetic field and the cycles were measured within the magnetic field range of ±2 T, which is a magnetic field high enough to saturate the magnetization in this direction. In Fig. 5 and Fig. 6 we show the hysteresis cycles at low fields for all samples of both series. The field step in the range of the magnetization reversal process was 2 Oe in order to resolve the coercive field with enough accuracy. The coercive field was calculated by taking the maximum value of the numerical derivative dM/dH.

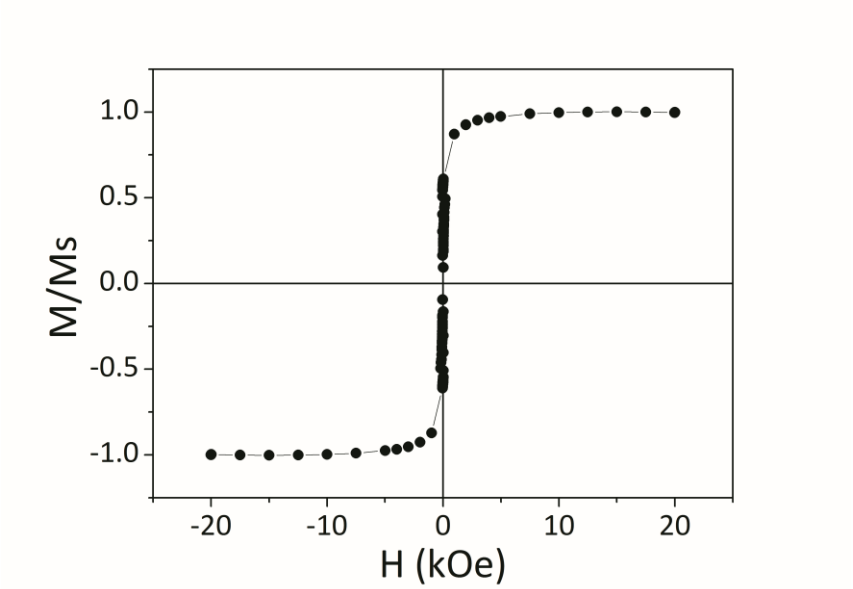

Fig. S4: Hysteresis loops for the 2.7-LMO sample at 4 K measured with an MPMS-SQUID.

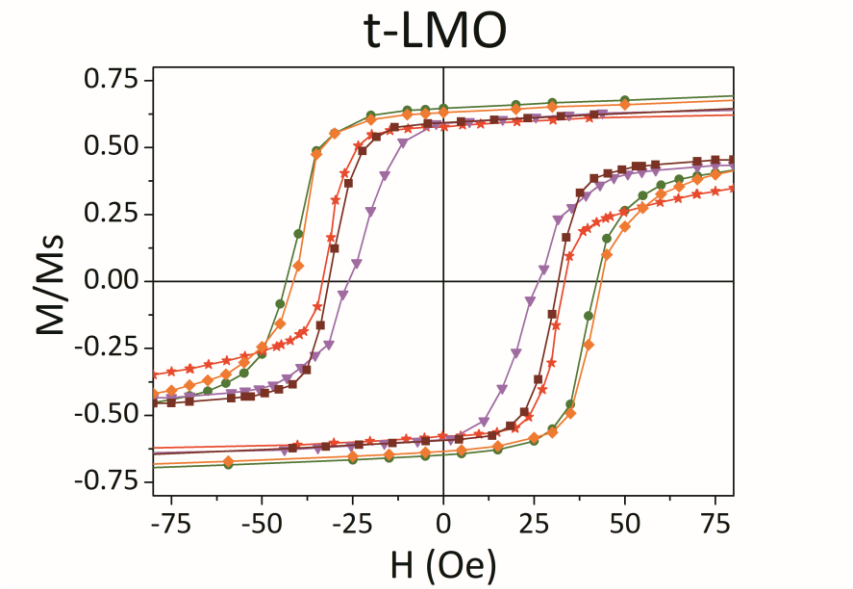

Fig. S5: Hysteresis loops for the t-LMO series at 4 K measured with an MPMS-SQUID. The samples with LMO capping layer thickness of 0 nm, 1.2 nm, 2 nm, 2,7 nm and 4,7 nm are denoted with circles, stars, triangles, squares and rhombus respectively.

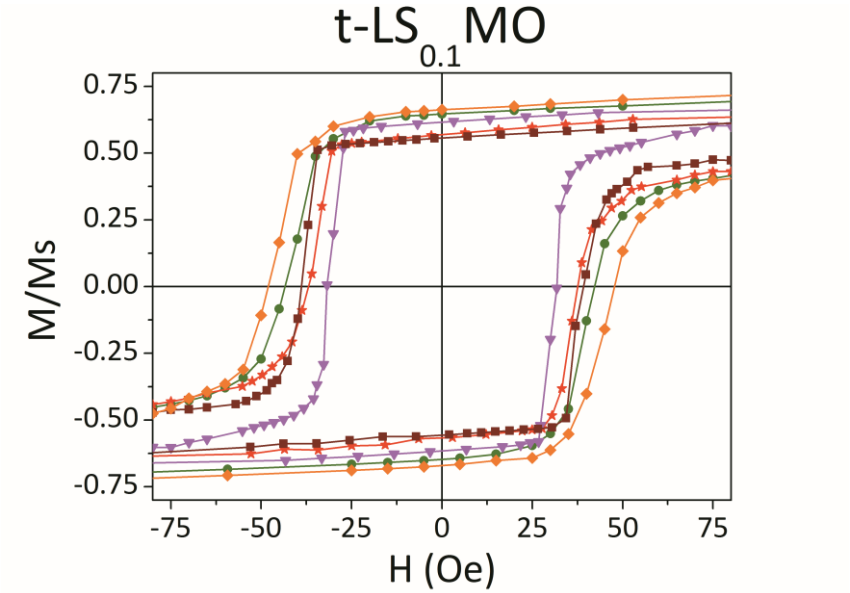

Fig. S6: Hysteresis loops for the t-$LS_{0.1}$MO series at 4 K measured with an MPMS-SQUID. The samples with $LS_{0.1}$MO capping layer thickness of 0 nm, 2 nm, 3.1 nm, 3.9 nm and 5.9 nm are denoted with circles, stars, triangles, squares and rhombus respectively.

Notes and references

[S1] J. Li, W. Peng, K. Chen, P. Wang, H-F. Chu, Y-F. Chen and D-N. Zheng. *Sci China-Phys Mech Astron*, **56**:2312–2326, 2013.

[S2] D. Pesquera, G. Herranz, A. Barla, E. Pellegrin, F. Bondino, E. Magnano, F. Sánchez and J. Fontcuberta. *Nat. Commun*. **3**:1189, 2012.